36E.0 IN-SITU CHARACTERIZATION OF MICROSTRUCTURAL EVOLUTION DURING SIMULATED ADDITIVE MANUFACTURING IN MODEL ALLOYS

Brian Rodgers (Mines)
Faculty: Amy Clarke (Mines)
Industrial Mentors: Edwin Schwalbach (AFRL), Neil Carlson (LANL)

This project initiated in Fall 2019 and is supported by a Multidisciplinary University Research Initiative (MURI) project funded by the Office of Naval Research (ONR) and the Office of Science, Basic Energy Sciences (BES). The research performed during this project will serve as the basis for a Ph.D. thesis program for Brian Rodgers.

36E.1 Project Overview and Industrial Relevance

Laser Powder Bed Fusion (L-PBF) Additive Manufacturing (AM) is an attractive technology for the manufacture of turbine and aerospace components. However, the processing effects of L-PBF on microstructural evolution are not well understood. This project will develop fundamental understanding of solidification phenomena under AM conditions in model alloys. Emphasis is placed on in-situ experimentation at the Advanced Photon Source (APS) at Argonne National Laboratory (ANL) and Dynamic Transmission Electron Microscopy (DTEM) at Lawrence Livermore National Laboratory (LLNL) with model alloys to understand the role of rapid solidification and processing history on microstructural development. Understanding solidification behavior during L-PBF could allow for the manufacturing of components like highly oriented, "single crystal" turbine components by AM.

The alloy systems chosen are two model ternary Ni-base superalloys with different Mo and Al contents, but identical equilibrium γ' volume fractions, and the Al-Ag system. The nickel alloys, R2 and R4, are single crystals of known orientation. R2 and R4 were chosen for their close resemblance to industrially relevant nickel-based alloys, while the Al-Ag system was chosen because it demonstrates strong chemical segregation behavior due to this system's shallow solidus and liquidus slopes.

36E.2 Previous Work – Simulations and Microstructural Characterization

In-situ experiments at the APS have been performed on alloys in the Al-Ag system and the R2 and R4 alloys. A summary of the alloy compositions and experimental matrix is provided in tables 36E.1 and 36E.2, respectively. The radiography of the melt pools has been compared against Rosenthal-type simulations of the melt pools. Aluminum melt pools tend to differ from ideal Rosenthal predicted shapes, due to high thermal diffusivity, invalidating the semi-infinite boundary assumption, while nickel melt pools have the same issue at low speed and power conditions, but mismatch due to convection at high speed and power conditions.

36E.3 Recent Progress

The top surface of all APS samples will be imaged and collectively reviewed for any features worth re-examining before sectioning begins. Sectioning will almost certainly damage features of interest on the top surfaces of the melt pools, so this process will ensure that no data is lost.

36E.3.1 Al-10Ag Microstructural Variants

Several microstructural variants in the as-solidified Al-10Ag have been observed. Most of them can be simultaneously observed in an image taken of a highly transient region in a re-rastered sample. Both the raster and the re-raster of this sample began as a conduction mode melt pool that transitioned to a keyhole mode pool as the edges of the sample became hotter, lowering the rate of heat extraction from the melt pool. The region around where the solid-liquid interface was when this occurred exhibits multiple microstructural variants in a small area, some of which are uniquely found here. **Figure 36E.1** displays an overview of the microstructures seen in the transition region and **Figure 36E.2** shows a higher magnification image of a microstructural variant seen only in this region. Regions A, B, and C all consist of columnar grains. Region B appears slightly different, because the ripples caused by fluid flow can be seen in the top surface. Region C has been more oxidized than regions A and B, due to the increased temperatures caused by keyholing. The area between regions B and C shows the most pronounced effects

Center Proprietary – Terms of CANFSA Membership Agreement Apply

of the transition between conduction and keyhole mode, with region D appearing as a cellular structure and region F having several pores ranging from 100s of nanometers to around a micron in diameter. Region E cannot be readily analyzed at the magnifications in **Figure 36E.1,** because the scale of the microstructure is so fine. This region cannot be readily put into a given category. There are two length scales of silver partitioning overlaid on one another, which may be a result of the re-melting and solidification from the re-raster, or an intrinsic behavior of this alloy at this position in gradient-velocity space. The coarser lines of increased silver content are also continuous throughout this region and connect regions B and C, as can be seen in **Figures 36E.1** and **36E.2**. It is tempting to initially describe the fine lines of silver rich material as lamellae, but this cannot be verified without viewing the structure from another angle via polishing into the centerline. There are also seaweed like features present in this region, which is sensible given the close proximity to the cellular structure.

More conventional microstructures have also been observed in the Al-Ag samples, such as columnar grains following the heat source. This can be seen in **Figure 36E.3**, which shows the columnar grain structure at the start and within the steady state regime of the raster. The angle of the columnar grains changes, because the shape of the melt pool and the thermal gradients are changing during the start of the raster, but are constant within some fluctuation in the steady state regime. It is also consistent with conventional welds that the angle of the columnar grains in the steady state regime is shallower than at the start of the raster, as the largest thermal gradient in the steady state regime is transverse to the raster direction for high raster speeds.

36E.3.2 Ni-Al-Mo Microstructures

All the Ni-Al-Mo microstructures imaged so far have either been fully dendritic, possibly cellular, or impossible to distinguish from top down imaging. It is believed that the microstructure is dendritic, due to the consistent orientation of the features, although this will become clearer with subsequent cross-sectioning and characterization of the melt pools. Some regions can be readily confirmed as being dendritic, due to their growth following crystallographic directions, rather than the maximum thermal gradient. **Figure 36E.4** shows an example of this behavior in an R4 raster, where the dendrites can be seen following the <100> orientation of the unmelted areas of the sample they nucleated on. Portions of the samples where the suspected dendrites are all vertical with their long axis orthogonal to the top-down viewing plane cannot be confirmed to be dendrites. Such features appear similar to a cellular solidification front, and can only be confirmed as dendritic with either crystallographic analysis methods or cross-sectioning and etching to view the dendrites orthogonal to their long axes. **Figure 36E.5** shows such a region in an R2 alloy that cannot be confirmed as dendritic without further analysis. Note how there are regularly spaced curved lines on the surface. This is caused by fluid flow. Other samples show straight lines, as shown in **Figure 36E.6**. These lines are believed to be slip lines from dislocation movement. If this is the case, then samples without dendrite growth in the top-down viewing plane can still be confirmed as fully dendritic.

A fully dendritic structure is not enough to confirm that a sample has retained a highly oriented “single crystal” structure after solidification, since columnar and equiaxed dendrites are both possible. Cross-sectioning, polishing into the middle, and analyzing the surface with EBSD will confirm whether a given sample has a columnar or equiaxed dendritic structure. Nevertheless, some of the sample can be confirmed to have nucleated new grain orientations not present in the initial solid before re-melting by the dendrite orientations, as seen in **Figure 36E.7**. Thus far, mismatched dendrite orientations indicating new grain nucleation have only been seen in spot melts and in the transient start region of rasters. Not having observed new grain orientation nucleation in the steady state regime of rasters is insufficient proof that it is not occurring, especially since not every sample has been imaged at the time of writing.

36E.4 Plans for Next Reporting Period

Ex-situ analysis of the APS samples will continue. Plans include:

- Further top-down imaging of as-solidified melts;
- More sophisticated melt pool and raster simulations using FLOW-3D to capture keyholing and convection and to understand local thermal conditions;
- Transverse and longitudinal imaging and EBSD of the rasters to provide crystallographic information;

Center Proprietary – Terms of CANFSA Membership Agreement Apply

- Imaging and EBSD of the center of spot melts with ‘longitudinal’ sections and overlapping spots to explore the role of complex thermal conditions on microstructure evolution.

Center Proprietary – Terms of CANFSA Membership Agreement Apply

36E.5 Figures and Tables

Table 36E.1: Compositions of alloys chosen.

	Ni (at%)	Al (at%)	Mo (at%)	Ag (at%)
R2	balance	6.6	1.9	N/A
R4	balance	2.8	22.2	N/A
Al-10Ag	N/A	balance	N/A	10
Al-18Ag	N/A	balance	N/A	18

Table 36E.2: Summary of laser parameters used in experiments at the APS. Pulse duration was 1 ms for all spot melts. Parameters for overlapping melts are shown with a forward slash between the parameters for each.

Alloy	Beam power [W]	Raster speed [m/s]	Notes
R2 [110], R2 [111], R4[100], R4 [110]	253.9	1.6	
	139.4	0.5	
	47.8	0.1	
	82.1/82.1	Spot melt	Edge of second pool intersects middle of first
	82.1/253.9	Spot melt	
R2 [110]	517.1	1.6	
	253.9	1	
R4 [100]	517.1	1.6	
	368.3	1.6	
	253.9	Spot melt	
Al-10Ag & Al-18Ag	282.5/282.5	0.1/0.1	Re-rasters with 100% overlap
	368.3/368.3	2/2	
	282.5	0.1	
	368.3	2	

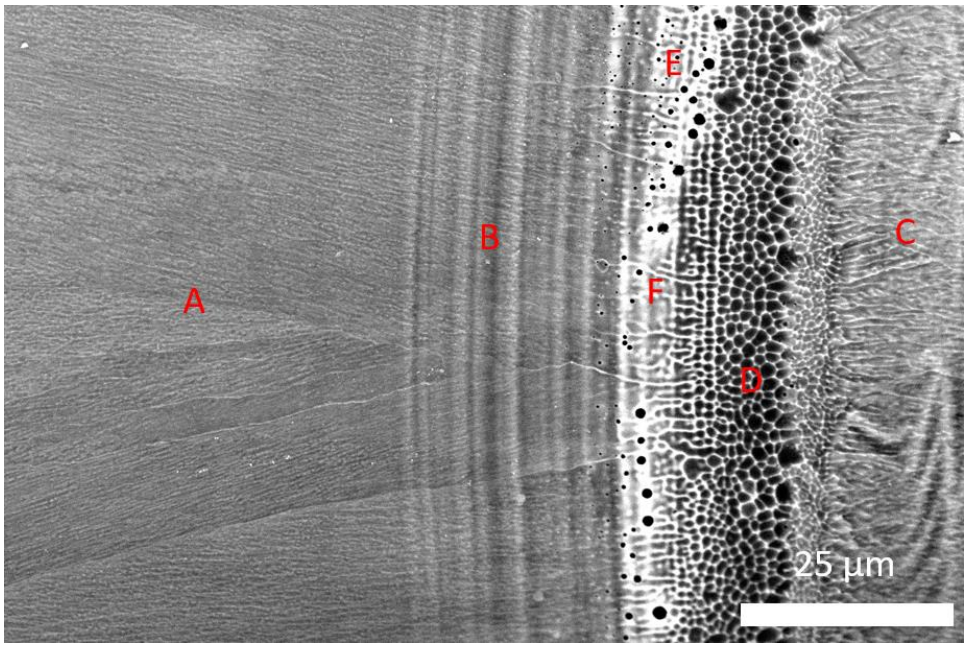

Figure 36E.1: Top-down SEM backscatter mode image of region in Al-10Ag re-rastered sample, with solid-liquid interface as present during conduction to keyhole mode transition. Labelled regions A-E are discussed in the text and region F appears in Figure 36E.2.

Center Proprietary – Terms of CANFSA Membership Agreement Apply

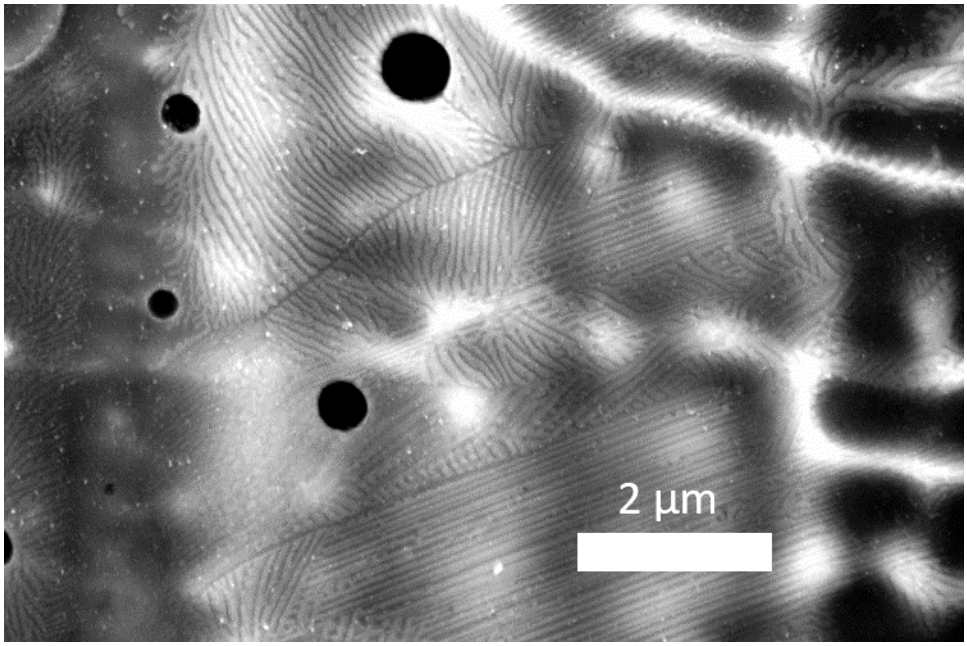

Figure 36E.2: Higher magnification image of region F in Figure 1.

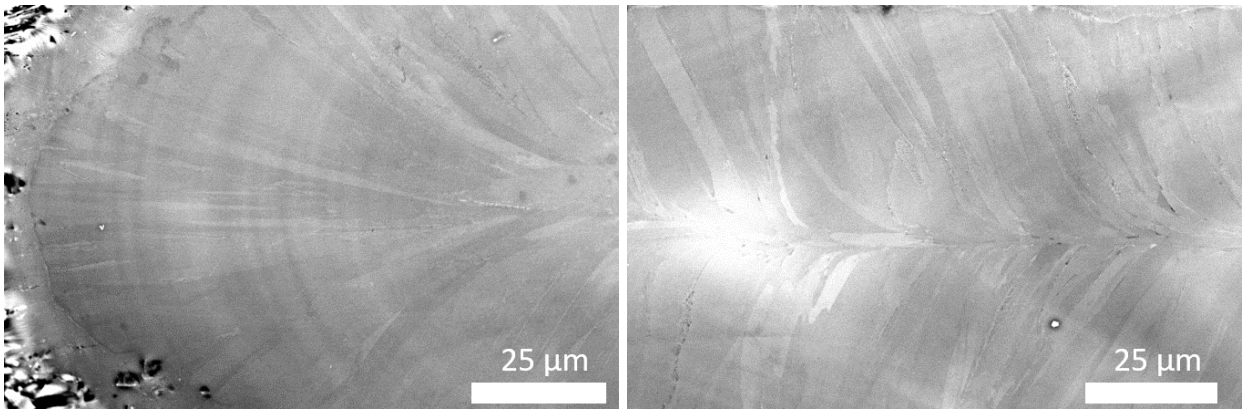

Figure 36E.3: Columnar grains in Al-10Ag at the start of the raster (left) and in the steady-state region (right), taken using SEM backscatter electron imaging.

Center Proprietary – Terms of CANFSA Membership Agreement Apply

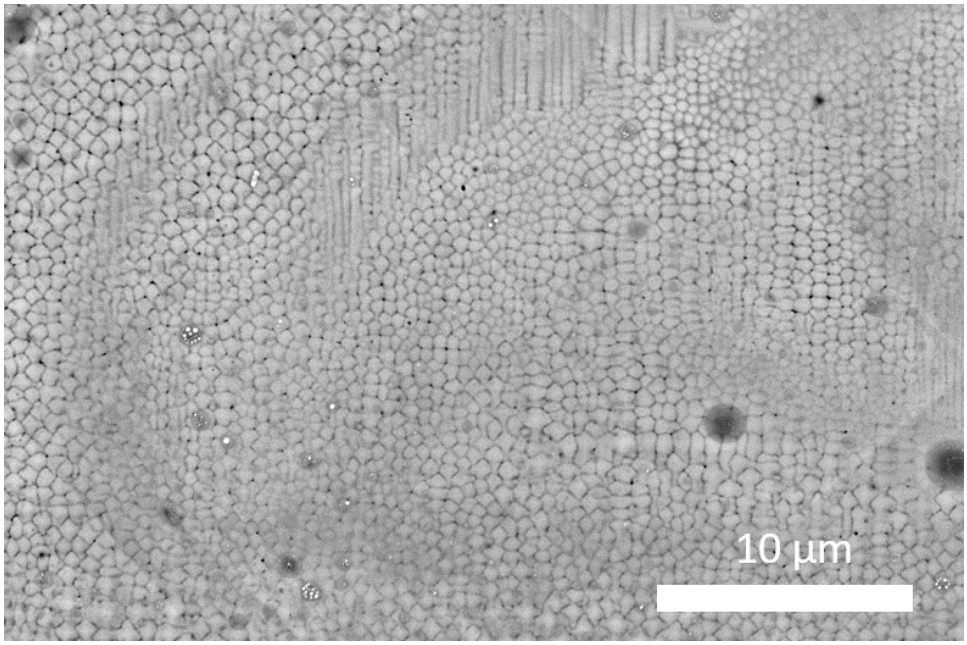

Figure 36E.4: Dendrites in rastered R4 alloy top surface, taken using SEM backscatter imaging.

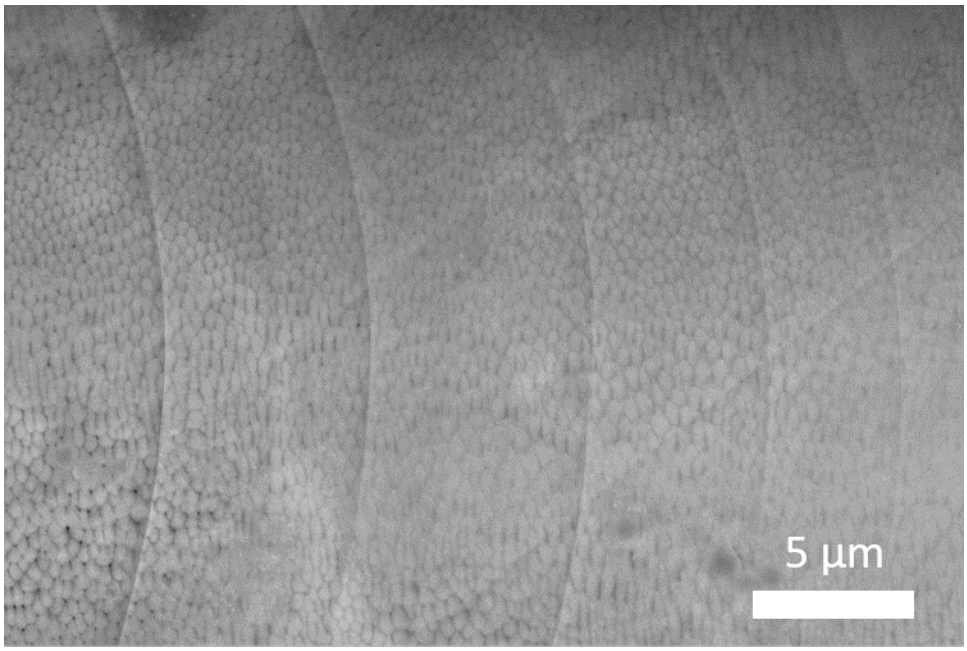

Figure 36E.5: Likely dendritic, possibly cellular structure in rastered R2 alloy top surface, taken using SEM backscatter imaging.

Center Proprietary – Terms of CANFSA Membership Agreement Apply

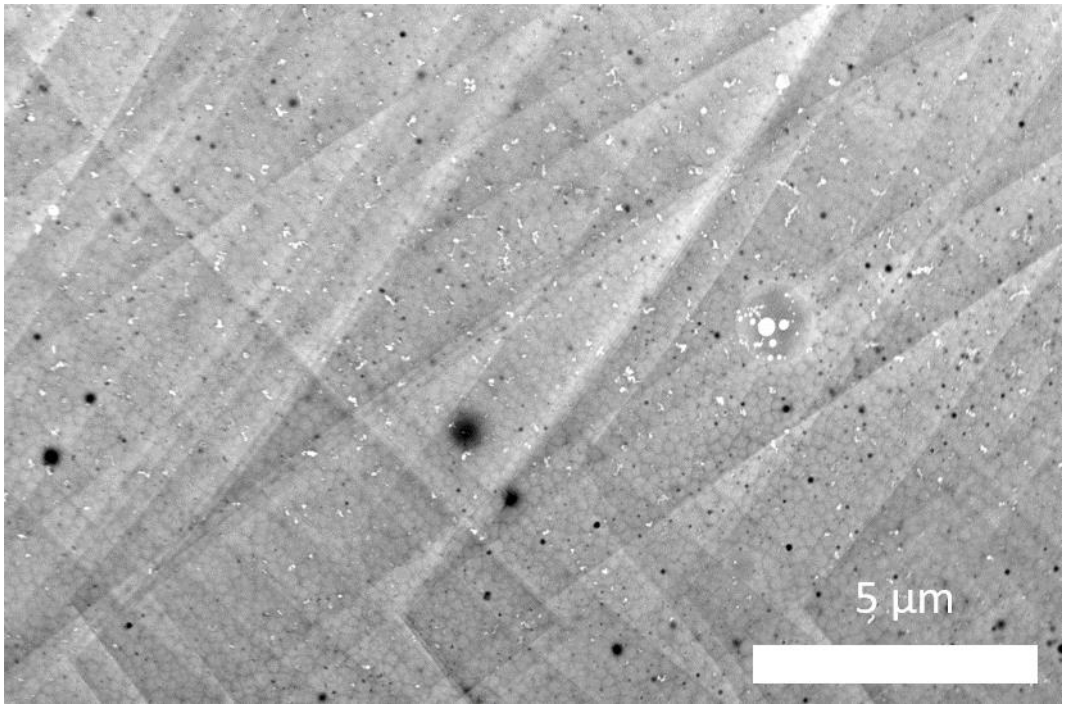

Figure 36E.6: Likely dendritic structure in rastered R4 alloy, with slip lines suggesting “single crystal”, taken using SEM backscatter imaging.

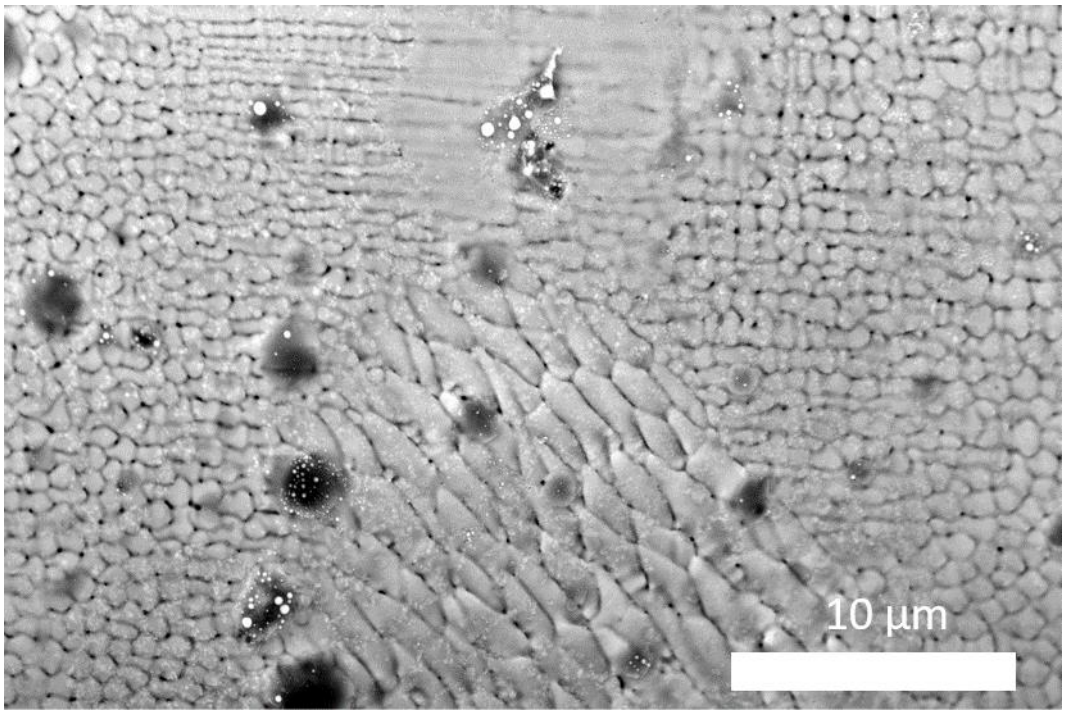

Figure 36E.7: New grain orientation nucleation in transient start region of R2 raster, taken using SEM backscatter imaging.

Center Proprietary – Terms of CANFSA Membership Agreement Apply